Talbot-Lau effect for atomic de Broglie waves manipulated with light

Andrey Turlapov,* Alexei Tonyushkin, and Tycho Sleator
Department of Physics, New York University, 4 Washington Place, New York, New York 10003, USA
(Received 3 November 2004; published 25 April 2005)

We have demonstrated the Talbot-Lau effect for atomic de Broglie waves in the time domain. This effect is based on Fresnel diffraction of matter waves from an incoherent source. In the experiment, de Broglie waves of atoms in a particular internal state have been manipulated and the resulting density directly imaged by resonant optical fields. These experiments allow us to probe the quantum dynamics of the atomic center of mass. We have also used this effect to create patterns in the density of the atoms with period as small as $1/10$ of the optical wavelength, demonstrating the potential application of this technique for atom nanofabrication.

DOI: 10.1103/PhysRevA.71.043612 PACS number(s): 03.75.Be, 42.50.Md, 42.82.Cr

I. INTRODUCTION

Observation of atom-optics phenomena has been facilitated by the existence of well-studied analogs in the optics of light. In conventional optics, diffractive self-imaging is possible in both the limiting cases of a spatially coherent and an incoherent source. Self-imaging of periodic structures in the two cases is known as the Talbot [1] and Lau [2] effect, respectively. In the Talbot effect, an optical *plane wave* illuminates a periodic grating. The grating image appears downstream due to Fresnel diffraction. In the Lau effect, monochromatic *spatially incoherent* light falls on a set of two parallel gratings separated by a known distance. At particular separations, illumination of some (or all) of the slits of the second grating is coherent and, thereafter, the second grating's image forms in the Fraunhofer diffraction zone. Also in the Lau setup, *Fresnel* diffraction causes formation of images at finite distances, similar to those observed in the Talbot effect. The appearance of these *Fresnel*-diffraction images can be referred to as the "Talbot-Lau effect."

For atomic de Broglie waves, the Talbot effect has been investigated with atomic beams manipulated by solid gratings [3,4] and also indirectly observed in a Bose condensate diffracted by optical fields [5]. Matter-wave Talbot-Lau effects have been demonstrated in a beam of atoms [6] and molecules [7] diffracted by material gratings.

We have studied the Talbot-Lau effect for de Broglie waves of atoms in a particular ground state. In contrast to Refs. [6,7], the absorptive gratings for the matter waves are pulses of resonant optical fields (so-called optical masks). Furthermore the experiment has been done in the time domain, with a cloud of cold thermal atoms. An optical mask [8,9] is a standing wave of light resonant to an open atomic transition. The period of this mask is $\lambda/2$, where λ is the optical wavelength. The standing-wave nodes act as slits in that an atom, initially prepared in a particular long-living energy level,[11] remains in this level only if located near a node during the mask pulse. Atoms in the bright zones are pumped into a different (ground) level and may be thought of as "absorbed."

Our experiments have allowed us to clearly observe several quantum effects involving the atomic center-of-mass motion, including a reduction of the fringe period from that predicted classically, as well as a shift in the position of the fringe maxima. We have also demonstrated that the Talbot-Lau effect may be used for creating density patterns of period $\lambda/2N$ for arbitrary integer N, which might be of interest for nanofabrication [10]. In the field of atomic-beam nanolithography, standing optical waves have been exploited for creating patterns of atomic density [11]. In the lithographic techniques demonstrated to date, the smallest density period has been limited to $\lambda/4$ [12].

The plan of the paper is as follows. The general concept of the time-domain Talbot-Lau effect is explained in Sec. II. The detection scheme and the experimental setup are described in Sec. III. The results are presented and analyzed in Sec. IV. In Sec. V, possible applications of the Talbot-Lau effect are discussed.

II. GENERAL PICTURE OF THE EXPERIMENT

The Talbot-Lau effect is a type of echo phenomenon. In an echo, an initial coherence created by some interaction washes out in a nondissipative way. Single or multiple repetition of the interaction restores the coherence (at least partially) at specific later times. Echoes are encountered in plasma physics [13], optics [14], condensed matter [15], and atomic physics [16]. A simple example of an echo is the "shadow effect," which is the appearance of shadows with various periodicity behind two parallel combs and is a purely geometrical phenomenon [17]. Some properties of our Talbot-Lau experiment can be understood in the language of the shadow effect. The schematic of the experiment is shown in Fig. 1.

At times $t=0$ and T, optical-mask pulses are applied to a thermal cloud of alkali-metal atoms, which are prepared in an initial hyperfine ground state. We shall consider only the atoms remaining in this state, and the term "density" will only refer to those atoms. The density structure of period $\lambda/2$ created by the first mask pulse quickly washes out due to

*Present address: Department of Physics, Duke University, Box 90305, Durham, NC 27708.

[1]For an alkali metal this might be a hyperfine ground level. For a noble-gas atom this could be an excited metastable level.

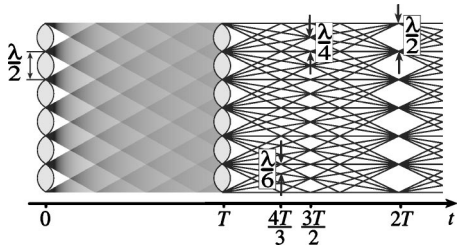

FIG. 1. Shadow effect for atoms manipulated with pulses of an optical mask. The horizontal axis is time, and the vertical is the coordinate along the mask. Black lines represent classical trajectories of the atoms in the initial ground state. The shaded region for $t<T$ represents a continuum of trajectories that result from the initial velocity distribution. Termination of some trajectories on the second mask represents "absorption" (optical pumping into a different ground energy level).

thermal motion (in Fig. 1, this is seen as spreading of the trajectories), and the density becomes uniform. Only atoms with particular discrete trajectories survive both pulses (solid lines in Fig. 1), and one may see that after the second pulse, at $t=2T$, the atoms rearrange into a structure with the initial period $(\lambda/2)$. More generally, at time $t=TM/N>T$, the density is modulated with period $\lambda/2N$, where the fraction M/N is in lowest terms (see Fig. 1). This instant is an echo time for the Nth spatial harmonic of density and its multiples.

The classical argument (shadow effect) correctly explains when a density structure forms and gives an upper bound to the period. Quantum physics manifests itself in the particular shape of the density distribution and in a reduction of the density period from that predicted from classical physics [17]. The quantum parameter of the experiment is the recoil phase $\omega_q T$, where $\omega_q=\hbar q^2/2m_{\text{atom}}$ is the recoil frequency, and $q=2\pi/(\lambda/2)$ is the absolute value of the mask grating vector. We refer to the time $2\pi/\omega_q$ as the Talbot time. By directly imaging the density, we have observed the effect of the recoil phase on the matter-wave diffraction and the small-period patterns in the density of atoms.

III. DETECTION TECHNIQUE AND EXPERIMENTAL SETUP

The real-time imaging technique and the apparatus are presented elsewhere [9] and are only briefly described here. Our experiments were done with atoms of ^{85}Rb initially prepared in the ground hyperfine level $F=3$. The mask standing wave is resonant to the $F=3\rightarrow F'=3$ transition ($5S_{1/2}\rightarrow 5P_{3/2}, \lambda=780$ nm). An excited atom is lost into the other ground hyperfine level $F=2$ with 4/9 probability. For a pulse of sufficient intensity and duration, atoms not located at the nodes will be depleted into the $F=2$ level.

For imaging the density at a particular time, we applied a "detection sequence," consisting of an optical mask, identical to the one described above (tuned to the $F=3\rightarrow F'=3$ transition), followed by a traveling-wave pulse tuned to the closed transition $F=3\rightarrow F'=4$ (see Fig. 2).

After the mask was applied, atoms left unpumped at the nodes were counted by observation of fluorescence in the

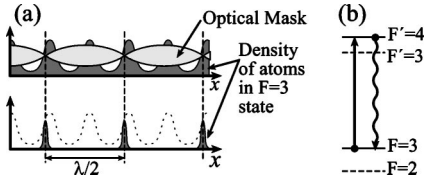

FIG. 2. Scheme for measuring a periodic atomic structure with an optical mask. (a) The effect of the standing-wave pulse on an initial periodic distribution of atoms in the $F=3$ state. In this example, the density period is $\lambda/4$. The shaded region shows the density of atoms in the $F=3$ hyperfine state before (upper curve) and after (lower curve) the standing wave pulse. (b) The scheme by which the number of atoms remaining in the $F=3$ state is measured. The wavy lines correspond to the fluorescent photons that are measured in the experiment.

traveling wave. The fluorescent signal is proportional to the density at the nodes just before the application of the imaging mask. To map out the density as a function of position, the initial density profile was reproduced and the measurement repeated with various locations of the detection mask node within the mask period $(\lambda/2)$.

This particular experiment is insensitive to the effects of gravity because the beams for the optical masks are arranged in a horizontal plane and, therefore, do not sense vertical motion.

The experimental setup is shown in Fig. 3.

The experiment was repeated every 40 ms. During the first 35 ms, atoms are trapped and cooled in a magneto-optical trap and in optical molasses, which gives a 1.4 mm cloud of 10^7 ^{85}Rb atoms at $\simeq 15\ \mu$K (the rms thermal velocity spread is $v^0_{\text{rms}}\simeq\sqrt{15\ \mu\text{K}/m_{\text{atom}}}\simeq 40\ \text{nm}/\mu\text{s}$). A 10 G magnetic field (for quenching the dark state of the mask $F=3\rightarrow F'=3$ transition) is turned on within 0.7 ms and the actual experiment starts 3 ms after the cooling fields are switched off. The standing wave for the optical mask is created by two traveling waves derived from the same laser and pulsed by two acousto-optic modulators (AOMs) driven by the same rf source. The duration of each mask pulse is 800 ns, which is much shorter than the the Talbot time $2\pi/\omega_q=65.4\ \mu$s and much longer than the excited state lifetime $1/\Gamma=27$ ns. The intensity at the mask's antinode is

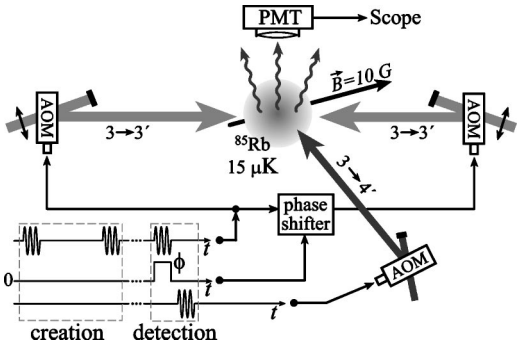

FIG. 3. Experimental setup. The lower part of the figure shows the timing of the rf pulses used to switch on the laser fields. The phase shifter is used to shift the nodes of the standing wave during the detection phase.

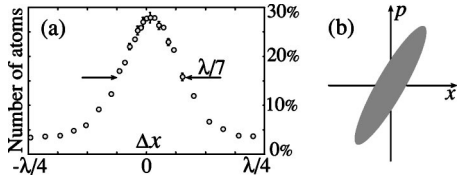

FIG. 4. (a) Number of atoms passing through the slits of two successive masks vs the shift between the masks. (The vertical scale is normalized to the number of atoms left after the application of only one mask pulse.) This profile is a measurement of the density distribution created by the first mask. Here and further, error bars represent confidence level of 68% and are statistical only. (b) Qualitative plot of the phase-space density created by a single mask pulse.

55 mW/cm^2=6.3I_{sat}, where I_{sat} is the average saturation intensity for the $F=3\rightarrow F'=3$ transition. The nodes of the detecting masks are shifted relative to the nodes of the creating mask by changing the phase of the rf feeding one of the AOMs. The readout field on the cycling $F=3\rightarrow F'=4$ transition is pulsed by a separate AOM. Fluorescent photons are captured by a photomultiplier tube (PMT).

IV. IMAGES OF DENSITY AND DISCUSSION

In the initial experiment, prior to observation of the Talbot-Lau effect, we illustrate the imaging technique: A *single* mask pulse created a density pattern, and the detection sequence was applied immediately after. In Fig. 4(a), we have plotted the number of atoms passing through these two masks vs the shift Δx between their nodes.

A significant number of atoms makes it through only if the slits of the two masks are nearly aligned. To calculate $w_{1/2}$, the upper bound for full width at half maximum localization of the atoms after a single mask pulse, one may neglect the atomic motion and assume that the image of Fig. 4(a) is a convolution of two identical Gaussian transmission functions. Then $w_{1/2}=\lambda/10$. The upper bound for the instrumental width of the mask *imaging* technique is also given by $w_{1/2}$.

The Talbot-Lau effect has been observed by applying pulses of the optical mask at $t=0$ and $t=T$, followed by the detection sequence at the (echo) time of interest. In Figs. 5(a)–5(c), we show the images of density taken at $t=2T$, $3T/2$, and $6T/5$, respectively.

The spatial period is $\lambda/2$, $\lambda/4$, and $\lambda/10$, respectively. This periodicity is consistent with the classical shadow effect (see Fig. 1) because in these experiments, the recoil phase $\omega_q T$ is a multiple of 2π.

Unambiguous quantum behavior of the atomic center of mass can be seen in the dependence of the density profile on the recoil phase $\omega_q T$. In the experiment, this phase is varied by the choice of T, the delay between the first and the second mask pulses. Figures 5(a), 5(d), and 5(e) show an image of the density for various $\omega_q T$ at time $t=2T$. Classically, at this time, the density period is expected to be $\lambda/2$. If $\omega_q T$ is chosen as $\pi/2$, the density period reduces to $\lambda/4$ as seen in Fig. 5(d). For $\omega_q T=\pi/3$, the density image contains primarily the third harmonic [see Fig. 5(e)]. Also, imaging the

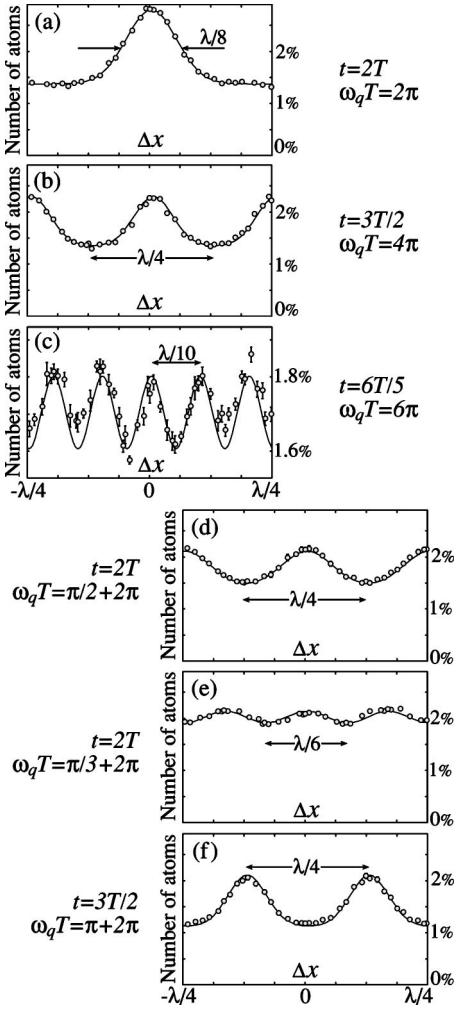

FIG. 5. Images of density generated in the Talbot-Lau effect: Number of atoms remaining in the initial hyperfine level after three mask pulses vs Δx, the shift between the two creating masks and the third, detecting, one. The circles are the data, and the curves are the theory. For (c), the vertical scale does not start from zero.

density at time $t=3T/2$ with recoil phase $\omega_q T=\pi$ (as opposed to 2π) yields a density pattern that is shifted by half of the mask period [compare Figs. 5(b) and 5(f)]. This shift in the density profile and the period reduction at $t=2T$ cannot be explained classically. We have modeled the Talbot-Lau effect by quantizing the atomic center-of-mass motion and assuming that the three optical mask pulses act as identical thin transmission gratings with Gaussian slits. By fitting the model to the data of Fig. 5(a), we have obtained slit width, peak transmission, and the background in the density image. These parameters were then used to model the data of Figs. 5(b)–5(f), and one can see from the figures that the model is in general agreement with the data.

Note that the density image of Fig. 4(a) is wider than the image of Fig. 5(a), even though the former is obtained by transmitting atoms through two successive masks only. One may calculate (either classically or quantum mechanically) that if the masks modulated the density instantaneously, the width of the echo image of Fig. 5(a) would be $\sqrt{3}$ times as wide as the image of Fig. 4(a). One can understand the nar-

rowness of the echo image by considering the *correlation* between momentum and coordinate created in each pulse of atom-mask interaction: During the interaction, a typical atom moves a distance comparable to the upper bound of the slit width $w_{1/2}$. Immediately after the first mask pulse, the atomic phase-space density looks like a tilted oval shown in Fig. 4(b). The width of image in Fig. 4(a) is due to the spatial extent of the *tilted* oval, while the localization of atoms in the echo is mainly due to the width of this oval "straight up," which explains the narrowness.

All images of the atomic density shown in Fig. 5 have significant background, which can be explained by two factors. First, these images appear as a result of transmission of atoms through three consecutive masks, each producing $\simeq 4\%$ background in the density relative to the $\simeq 45\%$ peak transmission [the estimates are based on the data of Fig. 4(a)]. This background in the individual mask's transmission explains $\simeq 60\%$ of the background in Fig. 5(a). The rest of the background could be due to partial incoherence of the transmission through the second mask pulse, which can be understood in terms of the shadow effect (Fig. 1): if an atom interacting with the second mask receives a recoil impulse due to spontaneous emission, its trajectory bends by a small random angle; as a result, at an echo time, the trajectory "misses" the intersection. The low contrast of the $\lambda/10$-period structures in Fig. 5(c) is primarily due to the fact that the spacing between peaks is on the order of the peak width. Note that, due to the nonzero instrumental resolution of the detection mask, the images of Fig. 5 have lower contrast than the actual density modulation at the echo times. In general, the contrast of both the images and the density modulation can be improved by using a mask with narrower slits. This can be achieved by increasing the duration or intensity of the mask as well as by employing an open transition with smaller branching into the initial energy level.

V. SUMMARY AND OUTLOOK

The reported Talbot-Lau setup can potentially be applied to gravitometry. For this, the optical masks would have to be arranged along the vertical direction. By mapping out the atomic density at, say, echo time $t=T(N+1)/N$ and varying T, one would measure how the Nth harmonic of density falls in the gravity field, allowing a precise measurement of the gravitational acceleration. An attractive feature of monitoring the highest possible harmonic is that the sensitivity of the interferometer would improve as N for a given maximum value of T. Such an interferometer would be similar to the one of Cahn *et al.* [18]. The main difference is in the detection scheme: The interferometer of Cahn *et al.* detects only the principal $(\lambda/2)$ harmonic of the density, while an interferometer with optical-mask detection would measure all the harmonics, and would therefore have a factor N increase in sensitivity to gravitational phase shifts in configurations where the Nth spatial harmonic is present.

The ability to create structures of period $\lambda/2N$ can be utilized for nanofabrication with an atomic beam. The experiment would have to be arranged in the space domain with two zones of atom-light interaction (as in Fig. 1 except that the horizontal axis would be the coordinate along the atomic beam), and the substrate would have to be placed in some echo plane. This technique would be particularly suitable for noble-gas atoms initially prepared in a metastable state. The high energy of the metastable state is released in the collision, locally damaging the substrate, which allows the transfer of density patterns onto a surface [19].

The atomic Talbot effect also can be used for creating density structures whose period is a fraction of the initial spatial modulation [4]. Unlike the Talbot effect, however, a deposition technique based on the Talbot-Lau effect does not require subrecoil collimation of the atomic beam, allowing a larger flux of atoms and, hence, shorter deposition times. Also, in the Talbot effect, if mask slits are not narrow enough, the desired small-period pattern appears on top of a larger-period structure.

ACKNOWLEDGMENTS

We are grateful to B. Dubetsky and P. Berman of the University of Michigan for useful discussions, and to E. Robinson and H. Stroke of NYU for comments on the manuscript. We acknowledge the financial support of the U.S. Army Research Office through the Grants No. DAAD19-00-1-0412 and No. DAAD19-99-1-0033, and the Packard Foundation.

[1] H. F. Talbot, Philos. Mag. **6**, 401 (1836).
[2] E. Lau, Ann. Phys. **6**, 417 (1948); F. Gori, Opt. Commun. **31**, 4 (1979).
[3] M. S. Chapman, C. R. Ekstrom, T. D. Hammond, J. Schmiedmayer, B. E. Tannian, S. Wehinger, and D. E. Pritchard, Phys. Rev. A **51**, R14 (1995).
[4] S. Nowak, Ch. Kurtsiefer, T. Pfau, and C. David, Opt. Lett. **22**, 1430 (1997).
[5] L. Deng, E. W. Hagley, J. Denschlag, J. E. Simsarian, M. Edwards, C. W. Clark, K. Helmerson, S. L. Rolston, and W. D. Phillips, Phys. Rev. Lett. **83**, 5407 (1999).
[6] J. F. Clauser and S. Li, Phys. Rev. A **49**, R2213 (1994); J. F. Clauser and S. Li, in *Atom Interferometry*, edited by P. R. Berman (Academic Press, San Diego, 1997).
[7] B. Brezger, L. Hackermüller, S. Uttenthaler, J. Petschinka, M. Arndt, and A. Zeilinger, Phys. Rev. Lett. **88**, 100404 (2002).
[8] R. Abfalterer, C. Keller, S. Bernet, M. K. Oberthaler, J. Schmiedmayer, and A. Zeilinger, Phys. Rev. A **56**, R4365 (1997); K. S. Johnson, J. H. Thywissen, N. H. Dekker, K. K. Berggren, A. P. Chu, R. Younkin, and M. Prentiss, Science **280**, 1583 (1998).
[9] A. Turlapov, A. Tonyushkin, and T. Sleator, Phys. Rev. A **68**, 023408 (2003).
[10] V. Sandoghdar, U. Drodofsky, T. Schulze, B. Brezger, M.

Drewsen, T. Pfau, and J. Mlynek, J. Mod. Opt. **44**, 1883 (1997).

[11] G. Timp, R. E. Behringer, D. M. Tennant, J. E. Cunningham, M. Prentiss, and K. K. Berggren, Phys. Rev. Lett. **69**, 1636 (1992).

[12] R. Gupta, J. J. McClelland, P. Marte, and R. J. Celotta, Phys. Rev. Lett. **76**, 4689 (1996).

[13] E. M. Lifshits and L. P. Pitaevskii, *Physical Kinetics* (Pergamon, Oxford, 1981).

[14] N. A. Kurnit, I. D. Abella, and S. R. Hartmann, Phys. Rev. Lett. **13**, 567 (1964).

[15] S. N. Popov and N. N. Krainik, Fiz. Tverd. Tela (Leningrad) **12**, 3022 (1970) [Sov. Phys. Solid State **12**, 2440 (1971)].

[16] T. W. Mossberg, R. Kachru, E. Whittaker, and S. R. Hartmann, Phys. Rev. Lett. **43**, 851 (1979).

[17] B. Dubetsky and P. R. Berman, in *Atom Interferometry* (Ref. [6]).

[18] S. B. Cahn, A. Kumarakrishnan, U. Shim, T. Sleator, P. R. Berman, and B. Dubetsky, Phys. Rev. Lett. **79**, 784 (1997).

[19] K. K. Berggren, A. Bard, J. L. Wilbur, J. D. Gillaspy, A. G. Helg, J. J. McClelland, S. L. Rolston, W. D. Phillips, M. Prentiss, and G. M. Whitesides, Science **269**, 1255 (1995).